

# Theoretical Interpretations of Low-Mass Dileptons \*

J. Wambach<sup>a</sup> and R. Rapp<sup>b</sup> †

<sup>a</sup>Institut für Kernphysik, Technische Universität Darmstadt,  
Schloßgartenstr. 9, D-64289, Darmstadt, Germany

<sup>b</sup>Department of Physics and Astronomy, State University of New York at  
Stony Brook, NY 11794-3800, USA

An overview is given of chiral symmetry restoration at finite temperature and baryochemical potential. Within hadronic models of the vector correlator its implications for low-mass dilepton spectra in ultrarelativistic heavy-ion collisions are discussed.

## 1. INTRODUCTION

In the limit of vanishing quark masses QCD exhibits an exact chiral symmetry, in which left- and right handed quarks decouple giving rise to conserved vector- and axialvector currents. In nature this limit is most relevant for the up- and down quark flavors, where masses are small compared to typical hadronic scales. To a somewhat lesser extent it also applies to the three-flavor case ( $N_f = 3$ ) which includes the strange quark. Chiral symmetry is fundamental to our understanding of light hadron masses where confinement seems to play a much lesser role. In the physical vacuum chiral symmetry is spontaneously broken. For the light meson spectrum representing elementary quark-antiquark modes (Fig. 1), this manifests itself in two ways:

- the appearance of (nearly) massless Goldstone particles (pion, kaon, eta).
- the absence of parity doublets, i.e. the splitting of scalar- and pseudoscalar, as well as vector- and axial vector mesons.

QCD sum rules relate meson masses to the quark condensate  $\langle \bar{q}q \rangle_0$ , an order parameter of spontaneous chiral symmetry breaking. For the  $\rho$ - and  $a_1$ -meson, for instance, one obtains in the large  $N_c$ -limit [1]

$$m_\rho^2 \approx \left[ \frac{448}{27} \pi^3 \alpha_s \langle \bar{q}q \rangle_0^2 \right]^{1/3} \quad m_{a_1}^2 \approx \left[ \frac{2816}{27} \pi^3 \alpha_s \langle \bar{q}q \rangle_0^2 \right]^{1/3}. \quad (1)$$

### 1.1. Chiral Symmetry Restoration

It is expected that chiral symmetry is restored at finite temperature,  $T$  and quark potential,  $\mu_q$ . The only reliable way to obtain the order of the transition, the critical

---

\*work supported in part by BMBF, NSF-PHY94-12309 and US-DOE under DE-FG02-88ER40388 .

†supported by the A.-v.-Humboldt Foundation as a Feodor-Lynen fellow.

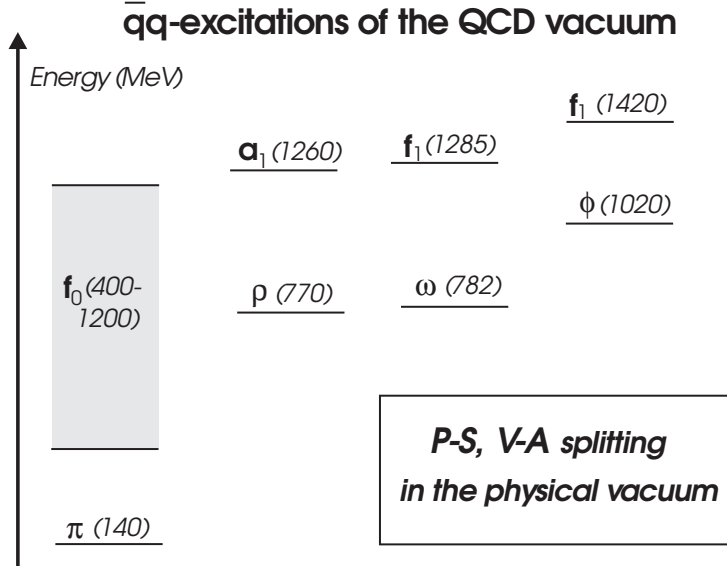


Figure 1. Low-lying spectrum of selected meson states.

temperature and the critical chemical potential is ab initio lattice simulations. While, at  $\mu_q = 0$ , results are available with  $T_c = 150 \pm 20$  MeV [2] there are difficulties for finite  $\mu_q$ . It has long been known that quenched QCD breaks down at non-zero  $\mu_q$  in that the transition takes place at  $\mu_q \approx m_\pi/2$  which is unphysical. Within random matrix models this failure is now understood as an inherent problem of the quenched approximation [3]. It is not clear at the moment whether an early onset of the transition truly holds in full QCD or if it reflects computational difficulties in the method employed for the simulation [4].

In spite of these difficulties with lattice QCD, model-independent results can be obtained at low temperatures and small baryochemical potential,  $\mu$ , from phenomenology. Considering the QCD-free energy

$$\mathcal{F} = -T \ln Z_{QCD} \quad (2)$$

where  $Z_{QCD}$  is the grand-canonical QCD-partition function, the condensate ratio can be expressed via the difference  $\delta\mathcal{F} = \mathcal{F} - \mathcal{F}_0$  as [5]

$$\frac{\langle \bar{q}q \rangle_{\mu,T}}{\langle \bar{q}q \rangle_0} = 1 - \frac{\partial \delta\mathcal{F}(\mu, T)}{\partial m_q}. \quad (3)$$

Here  $m_q$  denotes the quark masses, which act like the external field in a magnet. For a dilute gas of hadrons the ratio can be expressed in the two-flavor case as [6]

$$\frac{\langle \bar{q}q \rangle_{\mu,T}}{\langle \bar{q}q \rangle_0} \approx 1 - \sum_h \frac{\Sigma_h \rho_h^s(\mu, T)}{f_\pi^2 m_\pi^2} \quad (4)$$

where  $\Sigma_h \propto \partial m_h / \partial m_q$  denotes the Sigma-Commutator of hadron  $h$  and  $\rho_h^s$  its scalar density. For low temperatures and small baryon density degenerate nucleons and thermally

excited pions give the dominant contribution such that

$$\lim_{\mu \rightarrow 0, T \rightarrow 0} \frac{\langle \bar{q}q \rangle_{\mu,T}}{\langle \bar{q}q \rangle_0} \sim 1 - \frac{1}{m_\pi^2 f_\pi^2} \left( \Sigma_\pi \rho_\pi^s(T) + \Sigma_N \rho_N^s(\mu) \right). \quad (5)$$

Since  $\Sigma_\pi = m_\pi/2 = 69$  MeV and  $\Sigma_N = 45 \pm 8$  MeV are known experimentally, the dilute gas limit is well determined. The underlying physical picture is very simple. Whenever a hadron is created in the vacuum the  $\langle \bar{q}q \rangle$  condensate is changed locally since the condensate inside a hadron is different from that in the vacuum.

At  $\mu = 0$ , one can go a step further and derive a rigorous low-temperature expansion by means of chiral perturbation theory [7,5]. Taking the chiral limit  $m_\pi \rightarrow 0$  one obtains

$$\frac{\langle \bar{q}q \rangle_T}{\langle \bar{q}q \rangle_0} = 1 - x - \frac{1}{6}x^2 - \frac{16}{9}x^3 \ln \frac{T}{\Lambda} + \dots; \quad x = \left( \frac{T}{\sqrt{8}f_\pi} \right)^2 \quad (6)$$

where the temperature scale is set by  $\sqrt{8}f_\pi \sim 250$  MeV. While the  $T^2$ -and  $T^4$ -terms are model independent, model dependence enters at order  $T^6$  through the regularization scale  $\Lambda \sim 470$  MeV. The range of validity is restricted to  $T < 120$  MeV mostly because at this point heavier mesons start to enter.

For finite  $\mu$  the dilute gas expression (5) predicts a decrease of the condensate ratio which is linear in the vector density (for heavy particles the scalar density becomes equal to the vector density). At nuclear saturation,  $\rho_0 = 0.16/fm^3$ , this yields a  $\sim 35\%$  drop and naive extrapolation would indicate chiral restoration at  $\sim 3\rho_0$ . This clearly cannot be trusted, since the equation of state of nuclear matter greatly differs from that of a free Fermi gas at such high densities [8].

## 1.2. How to Detect Symmetry Restoration?

The principal tool for observing QCD phase transitions are ultrarelativistic heavy-ion collisions (URHIC's). In the study of chiral restoration the quark condensate  $\langle \bar{q}q \rangle_{\mu,T}$  is not directly measurable, however, and one has to look for other observables. It follows from chiral symmetry alone that, at the phase boundary, the scalar and pseudo-scalar correlators as well as the vector- and axialvector correlators must become identical. In principle, the observation of parity mixing can thus serve as a unique signal for chiral restoration. The study of phase transitions via correlators is known in condensed matter physics, as 'soft-mode' spectroscopy [1]. Here structural phase transitions in crystals are analyzed by measuring the frequency of low-lying lattice phonons ('soft modes'). A good example is  $SrTiO_3$  [9]. Above a critical a temperature  $T_c = 106$  K this crystal has cubical symmetry with a three-fold degenerate ' $R_{25}$ -mode'. Upon cooling this mode becomes soft with vanishing frequency at  $T_c$ . At this point the crystal undergoes a structural transition to a phase of tetragonal symmetry. As a consequence the three-fold degenerate soft mode splits into two modes one of which is two-fold degenerate. Upon further cooling the frequencies of these modes as well as their splitting increase. Obviously the low-lying phonon spectrum contains the information of the underlying symmetry change during a phase transition.

The direct QCD-analog is the behavior of the scalar- and pseudoscalar correlators. As manifest in the linear  $\sigma$ -model they are the carriers of chiral symmetry. As  $T_c$  is approached from above, the scalar ( $\sigma$ )- and pseudoscalar ( $\pi$ ) modes become soft and split

below  $T_c$  with the pion remaining massless in the chiral limit. The measurement in heavy-ion collisions of the scalar- and pseudoscalar correlators is difficult, however, since pions suffer strong final-state interactions. A better probe is the vector correlator since it couples to photons or dileptons which only undergo electromagnetic final-state interaction. Since the vector correlator in the vacuum is saturated by narrow 'resonances', the  $\rho$ ,  $\omega$  and  $\phi$ -mesons, the objective is then to study the spectral changes of vector mesons as a function of  $\mu$  and  $T$ . There are, in principle, two possibilities. As the scalar and pseudoscalar modes, also the vector modes could become 'soft' at  $T_c$ , giving rise to 'dropping masses'. This is the hypothesis of 'Brown-Rho scaling' [10] and would be a natural consequence of a direct relationship between the masses and the chiral condensate, as found in the vacuum (see eq. (1)). Brown-Rho scaling also explains qualitatively the rapid increase in entropy density across the phase boundary, seen in lattice QCD [11]. The second possibility is that the vector mesons remain massive at  $T_c$ , becoming degenerate with their axial partners. Support for this possibility comes from the fact that the masses of the  $\rho$ - and  $a_1$ -meson change as  $T^4$  [12] which is difficult to reconcile from a direct link between masses and the chiral condensate in the medium. Recall that the condensate ratio, in the chiral limit, decreases as  $T^2$ , for small  $T$ .

## 2. HADRONIC DESCRIPTIONS OF THE VECTOR CORRELATOR

### 2.1. General properties

The vector correlator in the vacuum is defined as the current-current correlation function

$$\Pi_{\mu\nu}^0(q) = i \int d^4x e^{iq\cdot x} \langle 0 | \mathcal{T} j_\mu(x) j_\nu(0) | 0 \rangle, \quad (7)$$

where  $\mathcal{T}$  denotes the time-ordered product and  $j_\mu$  is the electromagnetic current. For three flavors the current can be decomposed in terms of the quantum numbers of the relevant vector mesons as

$$j_\mu = j_\mu^{(\rho)} + j_\mu^{(\omega)} + j_\mu^{(\phi)}. \quad (8)$$

The corresponding quark content is

$$j_\mu^{(\rho)} = \frac{1}{2}(\bar{u}\gamma_\mu u - \bar{d}\gamma_\mu d), \quad (9)$$

$$j_\mu^{(\omega)} = \frac{1}{6}(\bar{u}\gamma_\mu u + \bar{d}\gamma_\mu d), \quad (10)$$

$$j_\mu^{(\phi)} = -\frac{1}{3}(\bar{s}\gamma_\mu s). \quad (11)$$

Current conservation implies a transverse tensor structure

$$\Pi_{\mu\nu}(q) = \left( g_{\mu\nu} - \frac{q_\mu q_\nu}{q^2} \right) \Pi(q^2), \quad \Pi(q^2) = \frac{1}{3}g^{\mu\nu}\Pi_{\mu\nu}(q). \quad (12)$$

The imaginary part of  $\Pi(q^2)$  is proportional to the cross section for  $e^+e^- \rightarrow \text{hadrons}$

$$R(s) = \frac{\sigma(e^+e^- \rightarrow \text{hadrons})}{\sigma(e^+e^- \rightarrow \mu^+\mu^-)} = -\frac{12\pi}{s} \text{Im}\Pi(s), \quad (13)$$

where  $\sqrt{s}$  is the total c.m. energy of the lepton pair. The vector mesons appear as resonances in the different hadronic channels carrying the respective flavor quantum numbers and the vector dominance model (VDM) quantitatively describes the resonant contribution to  $R(s)$  [13].

In a hadronic medium the vector correlator loses its simple vacuum Lorentz structure due to a preferred frame. In the grand canonical ensemble one has

$$\Pi_{\mu\nu}^{(\mu,T)}(q_0, \vec{q}) = i \int d^4x e^{iq\cdot x} \text{Tr} \left( e^{(-\hat{H} - \mu \hat{N})/T} j_\mu(x) j_\nu(0) \right) / Z \quad (14)$$

with separate dependence on energy and three-momentum. In addition, the longitudinal and transverse components of  $\Pi_{L,T}^{(\mu,T)}$  now become distinct. The same holds for the propagators

$$D_{L,T}^{(\mu,T)} = (q^2 - (m_V^0)^2 - \Pi_{L,T}^{(\mu,T)})^{-1}. \quad (15)$$

## 2.2. Theoretical approaches

At SpS energies the phase space in the final state is dominated by mesons (mostly pions) with a meson/baryon ratio of 5-7 [14]. In calculating modifications of vector meson properties through hadronic interactions, an obvious starting point is therefore a pure pion gas. For the  $\rho$  meson which in the VDM couples dominantly to two-pion states this implies a modification of the pion loop through the heat bath. The resulting thermal broadening has been calculated e.g. for on-shell  $\rho$  mesons [15] or within the hidden gauge approach [16] and found to be rather small. Accounting for off-shell propagation in e.g. resonant  $\pi\rho$ -scattering through the  $a_1(1260)$  meson gives rise to a  $\pi a_1$ -loop in the  $\rho$ -meson self energy. Especially for energies above 1 GeV this contribution might be substantial, depending, however, crucially on the choice of effective Lagrangian [17].

In spite of the scarcity of baryons in the hot hadron gas, they have a significant impact on the spectral properties of vector mesons, largely because of strong meson-baryon coupling. Several approaches have been put forward to determine these effects reliably. One approach starts from a low-density expansion of the vector correlator [13,18]. To leading order in density the vector correlator takes the form

$$\Pi_{\mu\nu}^{(\mu,T)}(x) = \Pi_{\mu\nu}^0 + (x) + \langle \pi | \mathcal{T} j_\mu(x) j_\nu(0) | \pi \rangle \rho_\pi(T) + \langle N | \mathcal{T} j_\mu(x) j_\nu(0) | N \rangle \rho_N(\mu) + \dots \quad (16)$$

and involves the pion- and nucleon Compton amplitudes. In the work of Steele et al. [18] these are obtained from data in a 'chiral reduction formalism' and automatically contain mixing of the vacuum vector- and axialvector correlators in the pion sector, as implied by chiral symmetry. The nucleon Compton amplitude is constrained from  $\gamma N$  photoabsorption data and the nucleon polarizabilities. In ref. [13] the  $T = 0$  limit of the low-density expansion (16) is considered. Then only the nucleon contributes and its Compton tensor is evaluated in the VDM combined with chiral  $SU(3)$  dynamics, based on an effective meson-baryon Lagrangian. In the heavy-baryon formalism, the vector meson-baryon amplitude is calculated for  $\rho$ ,  $\omega$ - and  $\phi$  meson scattering and significant modifications of the spectral properties are found (Fig. 2). Especially the  $\rho$  meson suffers substantial broadening, as density increases. The position of the 'pole mass' is not affected, however. The in-medium  $\omega$  meson also broadens and exhibits a downward shift of the 'pole mass'. The  $\phi$  meson spectral function is mostly affected in the sub-threshold region.

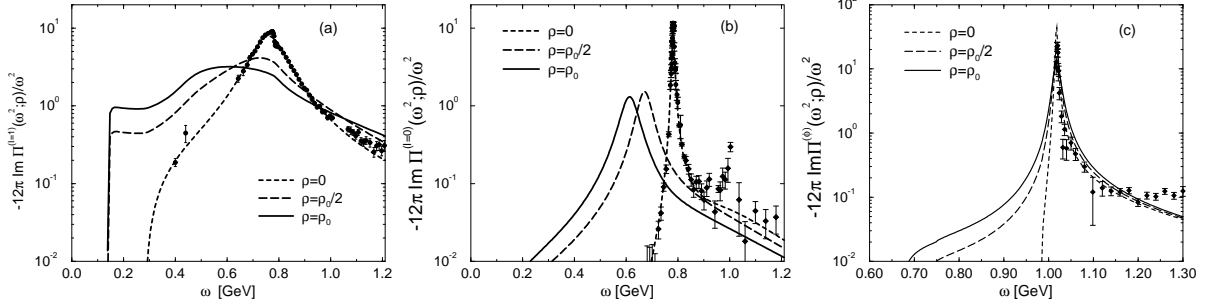


Figure 2. Modifications of the vector-meson spectrum [13]. Panels (a), (b) and (c) depict the  $\rho$ -,  $\omega$ - and  $\phi$  meson, respectively. The short-dashed lines denote the vacuum values, while the dashed (full) lines indicate the results at  $\rho_0/2$  ( $\rho_0$ ).

A second approach, which has been applied so far only for the  $\rho$  meson, starts from the well-known observation that pion propagation in the nucleus is strongly modified. A wealth of elastic  $\pi$ -nucleus scattering data has provided detailed understanding of the relevant physical mechanisms [19]. The dominant contributions originate from non-resonant and resonant  $\pi N$  scattering. Thus the pion self energy acquires large contributions from  $N$ -hole and  $\Delta$ -hole loops, giving rise to a momentum-softening of the pion dispersion relation. In the VDM it is therefore natural to account for this effect by replacing the vacuum two-pion loop with in-medium pions [20–22]. Gauge invariance is ensured by including appropriate vertex corrections. To lowest order in nucleon density this approach represents a pion cloud model for the nucleon Compton amplitude which coincides with that of ref. [18] and ref. [13] (in the latter case there are additional box diagrams). In addition to leading-order contributions in  $\rho_N$  there naturally emerge higher orders in density, most notably  $\rho_N^2$  terms. These correspond to two-nucleon processes of meson-exchange character and  $NN$ - and  $N\Delta$ -bremsstrahlung contributions. Besides the medium modifications caused by dressing the intermediate 2-pion states, direct interactions of the  $\rho$  meson with surrounding nucleons in the gas have to be considered. While elastic scattering,  $\rho N \rightarrow N \rightarrow \rho N$ , is kinematically strongly disfavored such a kinematic suppression will be much less pronounced with increasing energy of the resonance in the intermediate state. Indeed, there are at least two well-established resonances in the particle data table [23] which strongly couple to the  $\rho N$  decay channel, namely the  $N(1720)$  and the  $\Delta(1905)$ . This led to the suggestion [24] to consider  $\rho$ -like particle-hole excitations of the

Table 1  
Baryon resonances with appreciable decay width into  $\rho N$ .

$B^*$	$I(J^P)$	$\Gamma_{\rho N}$ [MeV]
$N(1520)$	$1/2(3/2^-)$	24
$\Delta(1620)$	$3/2(1/2^-)$	22.5
$\Delta(1700)$	$3/2(3/2^-)$	45
$N(1720)$	$1/2(3/2^+)$	105
$\Delta(1905)$	$3/2(3/2^+)$	210

type  $\rho N(1720)N^{-1}$  and  $\rho\Delta(1905)N^{-1}$ . In a more complete description other resonances with appreciable  $\rho N$  widths have been included [25–27]. These are listed in Tab. 1. The most simple version of the VDM overestimates the  $B^* \rightarrow N\gamma$  branching fractions when using the hadronic coupling constants deduced from the  $B^* \rightarrow N\rho$  partial widths. This is corrected for by employing an improved version of the VDM [28], which allows to adjust the  $B^*N\gamma$  coupling independently.

Combining the effects of pionic modifications and resonant  $\rho N$  scattering, the resulting  $\rho$ -meson spectral functions  $\text{Im}D^\rho = 1/3(D_L^\rho + 2D_T^\rho)$  are displayed in Fig. 3.

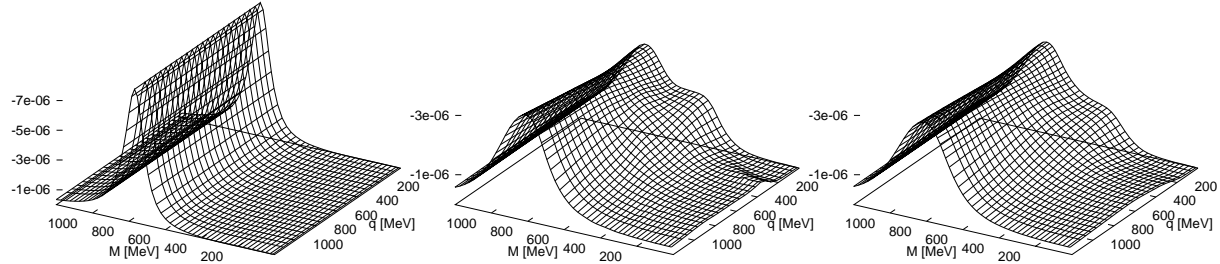


Figure 3. The  $\rho$ -meson spectral function [25,27] in the vacuum (left panel), at  $\rho_N = \rho_0, T = 0$  (middle panel) and at  $\rho_N + \rho_\Delta = 1.4\rho_0, T = 166$  MeV (right panel); notice that the vertical scale in the middle and right panel is reduced by a factor of 2.

One observes significant broadening especially at small  $q$  with a low-mass shoulder which originates from intermediate  $\Delta N^{-1}\pi$  states and resonant  $N(1520)N^{-1}$  excitations. As  $q$  increases the shoulder moves towards the  $M = 0$  line, which can be understood from simple kinematics. As seen from the right panel, temperature has little influence on the energy-momentum dependence and only provides an additional overall broadening.

### 2.3. Constraints from photoabsorption

An obvious constraint for models of  $\rho$ -meson propagation is photoabsorption in nuclei, for which a wealth of data exist over a wide range of energies. Real photons correspond to the  $M = 0$  line in the middle part of Fig. 3. Within the model discussed above, the total photoabsorption cross section per nucleon can be calculated straightforwardly. Taking the low-density limit,  $\rho_N \rightarrow 0$ , only terms linear in density contribute, representing the absorption process on a single nucleon. Two contributions have to be distinguished: (i) coupling of the photon to the virtual pion cloud of the nucleon, incorporated in the VDM via pion dressing; this contribution describes the background contribution the absorption process, as mentioned above; (ii) resonant contributions via the intermediate  $B^*$  resonances listed in Tab. 1.

Adjusting the model parameters to optimally reproduce the  $\gamma p$  data [27] yields results displayed in the left panel of Fig. 4. Photoabsorption on nuclei can be reproduced with similar quality. It is noteworthy that, in the nucleus, strength below  $m_\pi$  is obtained, which originates from two-nucleon processes via meson-exchange currents and is nothing but the 'quasi-deuteron tail' of the giant dipole resonance.

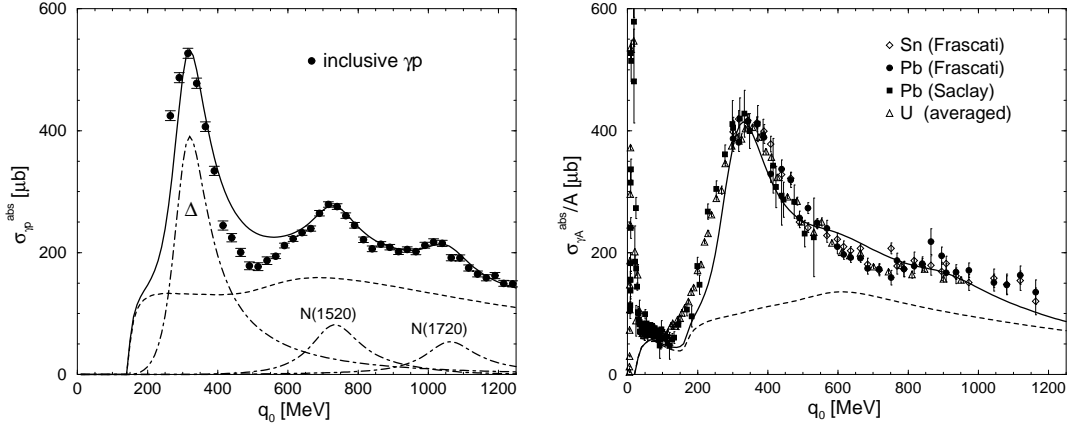


Figure 4. The photo absorption spectrum on the proton (left panel) and on nuclei (right panel) as obtained in ref. [27]. The dashed lines indicate the non-resonant background contributions. The data were taken from refs. [29-33].

#### 2.4. Comparison with Dilepton data

Constraining hadronic models via photoabsorption [18,27] gives confidence in extrapolations to the time-like region of dilepton production. For the  $\rho$  meson the dilepton rate is obtained as

$$\frac{dN_{\pi^+\pi^- \rightarrow l^+l^-}}{d^4x d^4q} = -\frac{\alpha^2 (m_\rho^0)^4}{3\pi^3 g^2} \frac{f^\rho(q_0; T)}{M^2} g^{\mu\nu} \text{Im}D_{\mu\nu}^\rho(q_0, q; \mu, T). \quad (17)$$

In the of model [25] most of the important processes discussed above have been included such that the  $\rho$ -meson propagator becomes

$$D_{\mu\nu}^\rho = D_{\mu\nu}^{\rho\pi\pi} + D_{\mu\nu}^{\rho NB^*} + D_{\mu\nu}^{\rho\pi a_1} + D_{\mu\nu}^{\rho KK_1} \quad (18)$$

and contains aside from the baryonic contributions also the most important parts from the pion/kaon gas.

To compare the theoretical rates with data, the space-time history of the heavy-ion collision has to be specified. There are several possibilities for modeling the collision. The most naive approach is a simple 'fireball' model [34,25], in which initial conditions in temperature and hadron abundances are obtained from transport model calculations. Assuming local thermal equilibrium as well as chemical equilibrium, the space-time history is then determined by a simple cooling curve,  $T(t)$ , from some initial time,  $t_i$ , up to the 'freeze-out time',  $t_f$ .

For SpS energies such cooling curves are available from transport theory [35] and can be easily parameterized. The time evolution of the hadron abundances is determined by chemical equilibrium and agrees well with transport model results. The observed spectrum is then obtained by integrating the 'local rate' (17) in time, accounting for the detector acceptance in addition. Results from [25,18] are displayed in Fig. 5. While the full results in the right panel [25] give a reasonable account of the observed spectra, especially in the region below the  $\rho, \omega$  mass, the results of ref. [18] fail to describe this region. The reason

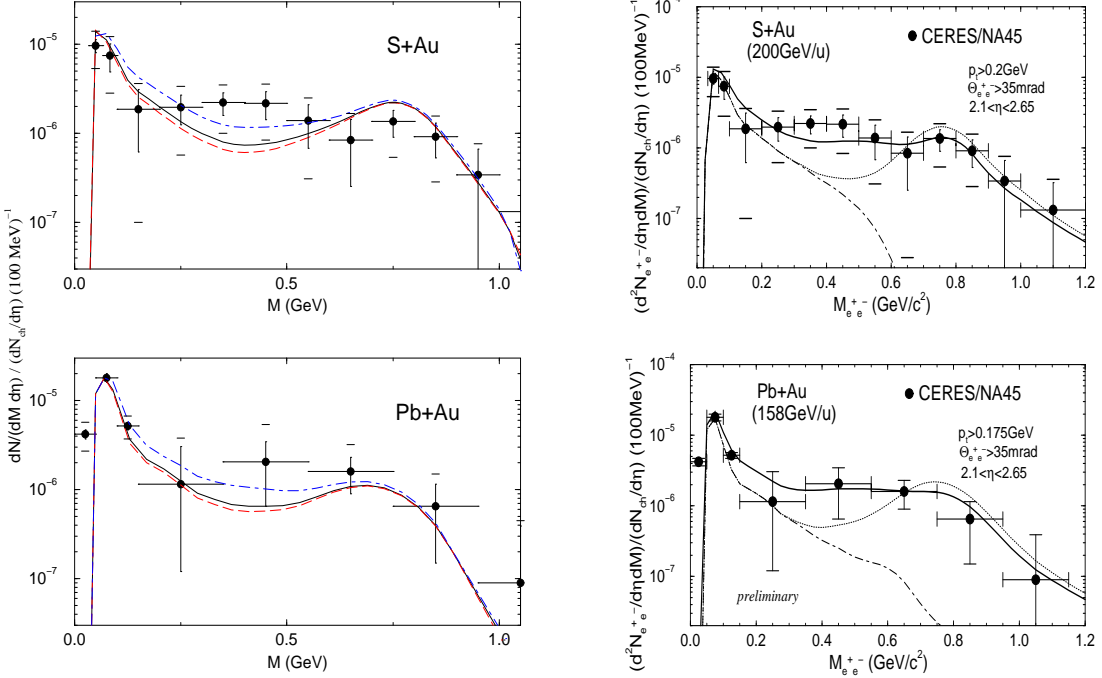


Figure 5. CERES Dilepton Spectra [36] employing the expanding fireball model of ref. [25] with in-medium dilepton rates from ref. [18] (full lines in left panels) and ref. [25] (full lines in right panels).

for this discrepancy between the two calculations is currently not completely understood.

The fireball model is rather crude and does not incorporate detailed flow dynamics. A more satisfactory description is provided by hydrodynamical simulations. In this case the 'local rates' (17) refer to a given fluid cell and can be directly implemented. So far, however, no results are available.

A third way is to supply transport calculations with rates obtained from in-medium vector-meson propagation. For the  $\rho$  meson this has been implemented in simulations using the *HSD* model for the transport [37]. Results have been obtained for both the CERES  $e^+e^-$ -measurement in Pb+Au collisions (left panel of Fig. 6) as well as the HELIOS-3  $\mu^+\mu^-$ -measurement of S+W collisions (right panel of Fig. 6). In both cases, the in-medium rates give an improvement in the comparison between theory and experiment and the overall description is quite satisfactory.

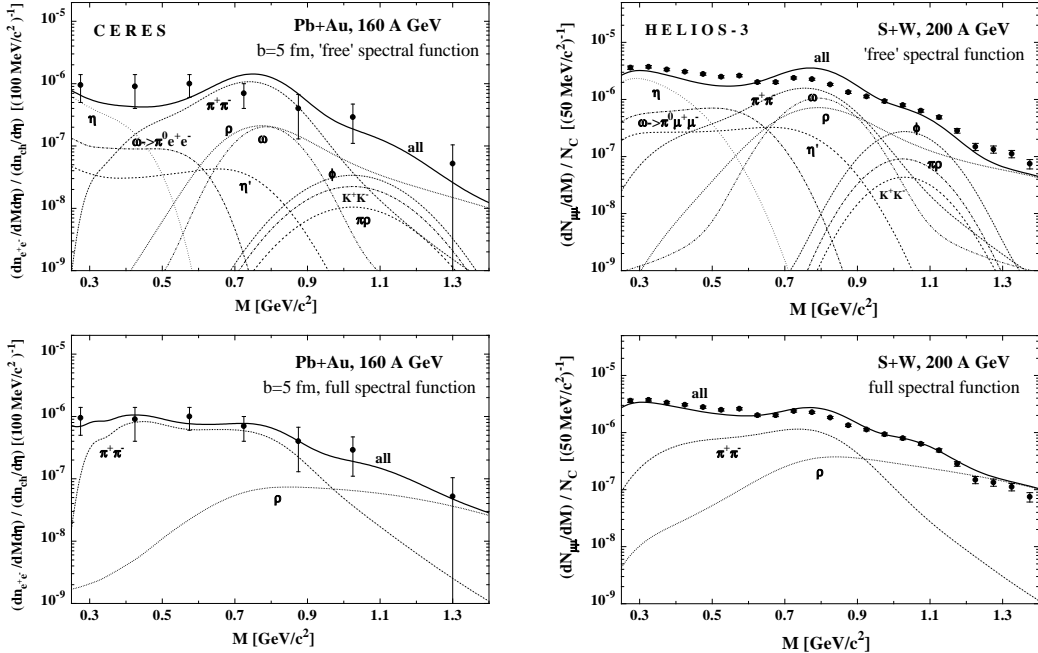


Figure 6. SpS Dilepton Spectra [36,38] employing the HSD transport model [37] using free (upper panel) and in-medium [25,27] (lower panel)  $\rho$ -meson spectral functions.

### 3. SUMMARY

Recent theoretical efforts in understanding the nature of chiral symmetry restoration at finite temperature and baryochemical potential and their implications for low-mass dilepton production in URHIC's have been discussed. While the onset of chiral symmetry restoration is well understood in the dilute gas limit, the approach towards the phase boundary within hadronic models remains a theoretical challenge. Here symmetry-conserving nonperturbative methods are called for. A unique signal for chiral symmetry restoration in URHIC's would be the observation of degenerate vector- and axialvector correlators. Such a mixing strictly follows from chiral symmetry but is difficult to detect. Only the vector correlator is accessible via electromagnetic probes.

The application of hadronic models to assess in-medium properties of vector mesons and their consequences for dilepton spectra have reached a degree of maturity such that realistic comparisons with data become meaningful. While some approaches inherently involve constraints from chiral symmetry [13,18], others lack an obvious connection to chiral symmetry emphasizing, however, input from hadronic phenomenology [34,25,27]. When supplemented by models for the space-time history of the collision, quantitative agreement between theory and experiment seems to emerge [25,37]. Further calculations

addressing more exclusive observables remain to be confronted with experimental data on a quantitative level.

## REFERENCES

1. T. Hatsuda, International Workshop on Soft Dilepton Production, August 20-22, 1997, LBNL and private communication.
2. E. Laermann, Nucl. Phys. **A610** (1996) 1c.
3. M.A. Stephanov, Phys. Rev. Lett **76** (1996) 4472.
4. A. Ukawa, these proceedings.
5. P. Gerber and H. Leutwyler, Nucl. Phys. **B321** (1989) 327.
6. G. Chanfray, M. Ericson and J. Wambach, Phys. Lett. **B388** (1996) 673.
7. J. Gasser and H. Leutwyler, Phys. Lett **B184** (1987) 83.
8. W. Weise, Nucl. Phys. **A610** (1996) 35c.
9. W. Gebhardt and U. Krey, 'Phasenübergänge und kritische Phänomene', (Vieweg & Sohn, Braunschweig/Wiesbaden, 1980) 183.
10. G.E. Brown and M. Rho, Phys. Rev. Lett **66** (1991) 2720.
11. F. Karsch, Nucl. Phys. **A590** (1995) 367c.
12. V.L. Eletsky and B.L. Ioffe, Phys. Rev. **D51** (1995) 2371.
13. F. Klingl, N. Kaiser and W. Weise, Zeit. Phys. **A356** (1996) 193; Nucl. Phys. **A624** (1997) 527.
14. J. Stachel, Nucl. Phys. **A610** (1996) 509c.
15. K. Haglin, Nucl. Phys. **A584** (1995) 719.
16. C. Song and V. Koch, Phys. Rev. **C54** (1996) 3218.
17. S. Gao and C. Gale, LANL e-print archive nucl-th/9711006.
18. J.V. Steele, H. Yamagishi and I.Zahed, Phys. Rev. **D57** (1997) 5605.
19. T.E.O Ericson and W. Weise, 'Pions and Nuclei', Clarendon, Oxford 1988.
20. M. Herrmann, B. Friman and W. Nörenberg, Nucl. Phys. **A560** (1993) 411.
21. M. Asakawa, C. M. Ko, P. Lévai and X. J. Qiu, Phys. Rev. **C46** (1992) R1159.
22. G. Chanfray and P. Schuck, Nucl. Phys. **A555** (1993) 329.
23. Particle Data Group, R.M. Barnett et al., Phys. Rev. **D54** (1996) 1.
24. B. Friman and H.J. Pirner, Nucl. Phys. **A617** (1997) 496.
25. R. Rapp, G. Chanfray and J. Wambach, Nucl. Phys. **A617** (1997) 472.
26. W. Peters, M. Post, H. Lenske, S. Leupold and U. Mosel, LANL e-print archive nucl-th/9708004.
27. R. Rapp, M. Urban, M. Buballa and J. Wambach, LANL e-print archive nucl-th/9709008 and Phys. Lett. **B** (1998) in press.
28. N.M. Kroll, T.D. Lee and B. Zumino, Phys. Rev. **157** (1967) 1376.
29. T.A. Armstrong et al., Phys. Rev. **D5** (1972) 1640.
30. A. Lepretre et al., Phys. Lett. **79B** (1978) 43.
31. J. Ahrens, Nucl. Phys. **A446** (1985) 229c;  
J. Ahrens et al., Phys. Lett. **146B** (1984) 303.
32. Th. Frommhold et al., Phys. Lett. **B295** (1992) 28; Zeit. Phys. **A350** (1994) 249.
33. N. Bianchi et al., Phys. Lett. **B299** (1993) 219; Phys. Rev. **C54** (1996) 1688.
34. G. Chanfray, R. Rapp and J. Wambach, Phys. Rev. Lett. **76** (1996) 368.

35. G.Q. Li, C.M. Ko and G.E. Brown, Nucl. Phys. **A606** (1996) 568.
36. G. Agakichiev *et al.*, CERES coll., Phys. Rev. Lett. **75** (1995) 1272;  
A.Drees for the CERES coll., in *Proc. of the Int. Workshop XXIII on Gross Properties of Nuclei and Nuclear Excitations*, Hirschegg 1995, eds. H. Feldmeier and W. Nörenberg, (GSI-Darmstadt 1995), p.151;  
Th. Ullrich for the CERES coll., Nucl. Phys. **A610** (1996) 317c.
37. W. Cassing, E.L. Bratkovskaya, R. Rapp and J. Wambach, LANL e-print archive nucl-th/9708020 and Phys. Rev. **C** (1998) in press.
38. N. Masera for the HELIOS-3 coll., Nucl. Phys. **A590** (1995) 93c.